Cement and Concrete Research 42 (2012) 511–525

Contents lists available at SciVerse ScienceDirect

Cement and Concrete Research

journal homepage: http://ees.elsevier.com/CEMCON/default.asp

Methods for determination of degree of reaction of slag in blended cement pastes

Vanessa Kocaba *, Emmanuel Gallucci, Karen L. Scrivener

Laboratory of Construction Materials, Ecole Polytechnique Fédérale de Lausanne, Lausanne, Switzerland

ARTICLE INFO

Article history:
Received 23 May 2010
Accepted 14 November 2011

Keywords:
Slag
Degree of reaction
SEM-BSE-IA-mapping
Calorimetry
Chemical shrinkage

ABSTRACT

To measure the degree of reaction of slag in blended pastes, five methods were studied. Selective dissolution and differential scanning calorimetry are shown to be unreliable, SEM-BSE-IA-mapping is time consuming, but does provide good results with a reasonable degree of precision. The difference in cumulative calorimetry and chemical shrinkage curves of slag blends in comparison to blends with inert filler shows potential to isolate the reaction of the slag. These methods have the advantage of being continuous, techniques with good precision, but the absolute heat of hydration, or contribution to chemical shrinkage of any particular slag is not known. Calibration of the calorimetry technique with SEM-BSE-IA-mapping seems to be a promising method to understand and quantify the degree of reaction of slag.

1. Introduction

The need to limit the environmental impact of cementitious materials and to dispose of by-products such as slag leads to the increasing use of supplementary cementitious materials, either preblended with ground clinker or added during fabrication of concrete. It is well known that these SCMs react more slowly than cement clinker and this limits the levels of substitution, due to the need for adequate properties at early ages. In order to better understand the factors affecting the rate of reaction of SCMs, it is essential to have a good method to evaluate the degree of reaction of these materials independently from the degree of reaction of the clinker component.

The classic method for measurement of degree of reaction is from the bound water content [1–3]. However this depends on assumptions about the quantity of water bound by the hydrate phases. The following equations illustrate the amount of bound water depends on the phase reacting (number of reacting water molecules are shown in bold).

Hydration of tricalcium silicate:

$$C_3S + (\mathbf{3-x+y})\mathbf{H} \rightarrow C_x-S-H_y + (3-x)CH \quad (1)$$

Hydration of dicalcium silicate:

$$C_2S + (\mathbf{2-x+y})\mathbf{H} \rightarrow C_x-S-H_y + (2-x)CH \quad (2)$$

Hydration of tricalcium aluminate with calcium sulphate:

$$C_3A + 3C + \mathbf{32H} \rightarrow C_6A_3H_{32}(\text{ettringite}) \quad (3)$$

or

$$C_3A + 3CH_2 + \mathbf{26H} \rightarrow C_6A_3H_{32}(\text{ettringite}) \quad (4)$$

$$2C_3A + C_6A_3H_{32} + \mathbf{4H} \rightarrow C_4AH_{12}(\text{monosulfoaluminate}) \quad (5)$$

$$C_3A + \mathbf{6H} \rightarrow C_3AH_6 \quad (6)$$

Hydration of tetracalcium aluminoferrite:

$$C_4AF + 3CH_2 + \mathbf{30H} \rightarrow C_6A_3H_{32} + CH + FH_3 \quad (7)$$

$$C_6A_3H_{32} + 2C_4AF + \mathbf{12H} \rightarrow 3C_4AH_{12} + 2CH + 2FH_3 \quad (8)$$

$$C_4AF + \mathbf{10H} \rightarrow C_3AH_6 + CH + FH_3 \quad (9)$$

It can be seen that even for typical Portland cements, the stoichiometry of the hydration reactions is not precisely known. In particular it is known that the amount of water bound in the C–S–H varies with temperature and that the overall water combined by the aluminate containing phases changes over time due to sulfate and carbonate contents, and to the extent of ferrite reactions; all of which remain unclear [4,5].

When slag is present, the use of bound water as a measure of the overall degree of hydration becomes completely unreliable due to the unknown stoichiometry of the reactions, which will also depend on the slag composition and will be further complicated by the changes in C–S–H composition which occur in blended materials.

In recent decades, the use of image analysis [6] and quantitative X-ray diffraction [7–10], particularly coupled with Rietveld analysis, has proven to be effective for the measurement of the degree of reaction of clinker in cement pastes. There is good agreement between these techniques [8,11] which can also be used to compute the degree of reaction of the clinker components. In principle, these methodologies can

* Corresponding author.
E-mail address: Vanessa.Kocaba@saint-gobain.com (V. Kocaba).

0008-8846/$ – see front matter © 2011 Elsevier Ltd. All rights reserved.
doi:10.1016/j.cemconres.2011.11.010

also be used to measure the degree of reaction of the clinker component in blended systems.

Measurement of the degree of reaction of the SCM itself poses new challenges. The reactive part of most of these materials is amorphous, so it cannot be measured directly by X-ray diffraction but the homogeneous regions of slag can be detected and quantified by image analysis [12,13].

Several authors [14–20] have used selective dissolution methods (discussed in more detail below) whose intention is to dissolve the reaction products and unhydrated cement, leaving the unreacted slag. It has also been suggested [1,21] that differential thermal analysis (DTA) can be used to recrystallise slag at high temperatures (between 800 °C and 1100 °C). Some studies [22–24] have reported the use of cumulative heat obtained from isothermal calorimetry or the volume changes associated with chemical shrinkage. The advantage of these methodologies is that they are continuous and in-situ. The problem, however, is to convert the resulting curves to a degree of slag reaction.

This paper evaluates five methods to measure the degree of reaction of slag in blended pastes:

- Selective dissolution.
- Recrystallisation of slag from differential scanning calorimetry.
- Image analysis from BSE grey level images and EDS mappings from SEM.
- Cumulative heat evolution curves from isothermal calorimetry.
- Chemical shrinkage curves.

2. Previous work on the selected methods

2.1. Selective dissolution

This method is based on a preferential chemical dissolution of the hydration products and unhydrated cement [14–20] leaving the unreacted slag. In recent studies [19,20,25] a modified method was presented which was used in this work. Its principle is based on the assumption that clinker phases, their hydrates and the hydrates formed from the slag are mostly dissolved leaving the unhydrated slag as a residue. Ethylenediaminetetraacetic acid (EDTA), triethanolamine and sodium hydroxide solution are claimed to dissolve the clinker minerals and calcium sulphate, at pH 11.5, without a notable dissolution of the slag. Precipitation of silica and hydroxides is avoided by the addition of sodium hydroxide [14]. By means of a comparative study, Luke and Glasser [17] concluded that this EDTA based modified method of Demoulian [14] was the most suitable.

Previous researchers already noted that in fact the dissolution is incomplete. Taylor and Mohan [26] noted that large corrections must be made for incomplete dissolution of others phases, and estimated the error on the results to be about ±10%. In previous studies [27,28], the authors mentioned that besides slag, some cementitious phases (such as periclase and aluminate) and hydrated phases from slag (hydrotalcite) are not dissolved either by selective dissolution. In addition, Goguel [29] identified high amounts around 2 to 5% of undissolved cement hydration products.

2.2. Differential thermal analysis/differential scanning calorimetry

One of the oldest method to determine the glass content of slag is thermal analysis: differential thermal analysis (DTA) is the most used [21,30–34] with differential scanning calorimetry (DSC) [35] as an alternative. The first reversible exothermic peak in the temperature range 700–800 °C corresponds to the glass-transition temperature T_g. This transition temperature mainly depends on thermal history (cooling rate) and structure [36]. The two exothermic peaks with well-defined maxima in the range 925–1040 °C are attributed to the devitrification process. Using X-ray diffraction, these peaks were respectively assigned to merwinite (metastable phase) and melilite with minor components (such as larnite) [21,35].

It has been suggested that quantification of the peaks could be used to determine the degree of reaction of slag [1,21,37,38]. However, it is not always easy to isolate the contribution of anhydrous slag because of the background contribution.

2.3. Backscattered electron images analysis

Backscattered electron images (BSE/IA) allow phases to be identified according to their brightness, which depends on their average atomic number. Several studies have shown that the amount of unreacted cement measured this way corresponds well to the other independent measures of degree of hydration [39]. For a cement paste, Scrivener et al. [39] showed that ten fields at 400× magnification were sufficient to give a standard error of around 0.6%. Another statistical analysis [40] showed that a set of 30 images at 200× magnification gave a mean with an error of <0.2% in pastes and mortars. In this study [40] 50 fields were analysed at 200× magnification to obtain the lowest reasonable standard error. More recently, it was shown that the degree of hydration of cement measured by BSE/IA agrees well with that obtained by X-ray diffraction–Rietveld analysis [8].

The amorphous component of a given slag source generally has a homogeneous grey level, which should allow it to be identified by image analysis. Brough and Atkinson [12,13] used this to quantify the degree of reaction of slag in alkali-activated cement mortars. Therefore, BSE/IA seems to have good potential for slag blended systems.

2.4. Isothermal calorimetry

Isothermal calorimetry is mainly used to the heat released by the hydration reaction at early ages (first 24 h) while at longer times the heat output is quite low and hardly resolved from the background. Nevertheless previous researchers [41,42] suggested that following the long term heat evolution of blended pastes could allow the reaction of supplementary cementitious materials to be monitored. This technique is investigated in the present study.

2.5. Chemical shrinkage

Measurement of chemical shrinkage is based on the fact that the volume occupied by the hydration products is lower than that of the reactants. This is due to the fact that "water" has a lower specific volume when bound to a solid than when free in a liquid as reflected in the following equation:

$$V_{\text{cement}}(t=0) + V_{\text{water}}(t=0) > V_{\text{hydrates}}(t) \quad (10)$$

Where:

$V_{\text{cement}}(t=0)$: initial volume of cement;
$V_{\text{waters}}(t=0)$: initial volume of water;
$V_{\text{hydrates}}(t)$: volume of hydrates at time t.

The method chosen here is dilatometry based on the protocol developed by Geiker [24] and optimised by Costoya [43].

3. Materials and methods

3.1. Materials

The chemical compositions of the three cements and the two slags investigated are given in Table 1.

Table 1
Chemical composition of raw materials from X-ray fluorescence analysis.

Oxides	Cement A	Cement B	Cement C	Slag 1	Slag 8	Error
SiO_2	24.68	20.51	21.01	36.61	34.60	0.40
Al_2O_3	2.11	5.10	4.63	12.21	19.98	0.20
Fe_2O_3	0.43	3.33	2.60	0.85	0.47	0.10
CaO	68.67	61.29	64.18	41.59	32.48	0.40
MgO	0.58	2.82	1.82	7.18	9.17	0.10
SO_3	1.82	2.78	2.78	0.63	1.99	0.10
K_2O	0.06	1.40	0.94	0.28	0.78	0.04
Na_2O	0.17	0.24	0.20	0.18	0.16	0.03
MnO	0.01	0.05	0.03	0.14	0.06	0.01
TiO_2	0.05	0.19	0.14	0.35	0.67	0.01
P_2O_5	0.45	0.37	0.40	0.01	0.01	0.01
LOI	0.97	1.94	1.26	−0.03	−0.37	0.10
Na_2Oeq	0.22	1.16	0.81	0.36	0.67	0.07
CO_2	1.30	0.80	1.40	–	–	0.20
Total	100	100	100	100	100	–

3.2. Mix design and sample preparation

60%wt of cement and 40%wt of slag were preblended together for 5 h in a TURBULA shaker–mixer to ensure a good homogenisation of the mixture. Hydrated mixes were prepared at room temperature (20 °C) with deionised water. To avoid any scattering of measured data due to the quantity of mixed components, 160 g of paste were mixed in one batch to provide all the specimens for all analyses (calorimetry, chemical shrinkage, SEM and XRD). The cementitious pastes were mechanically mixed (IKA LABORTECHNIK RW20.n) at a speed of 500 rpm for 3 min, stopped for 2 min and finally mixed at 2000 rpm for 2 min. The neat cement pastes were prepared at a water to cement ratio (by weight) of 0.40 while the water to cement ratio of the blend pastes was adapted so that the volume to water binder remains the same as for the pure cement; this corresponds to a 0.42 water to solids ratio by weight for the 40% slag blend.

The hydration was stopped at different ages ranging from a few hours to several days. At early ages the hydration was stopped by freeze-drying. The sample was frozen at −80 °C in a cold mixture of solid CO_2 and liquid ethanol and subsequently dried by sublimation. At later ages, the water in older samples was removed by solvent exchange in isopropanol for one week. Once dried, all specimens for SEM examination were impregnated under vacuum in an epoxy resin (EPOTEK 301) and carefully polished with decreasing grades of diamond powders down to 1/4 μm.

3.3. Selective dissolution

Selective dissolution was used according to the protocol given by Luke and Glasser [17] and recently used by Dyson [25]. The following solutions were used:

- 0.05 M ethylenediaminetetraacetic acid (EDTA);
- 0.1 M Na_2CO_3 solution;
- a 1:1 solution (by volume) of triethanolamine:water mixture;
- 1.0 M NaOH.

The different steps are the following:

- 125 mL of EDTA and 125 mL of Na_2CO_3 were mixed together in a one litre conical flask.
- 12.5 mL of the triethanolamine/water mixture was then added and the pH was checked to be 11.6 ± 0.1. If necessary, the pH was adjusted by addition of small quantities of 1.0 M NaOH.
- A 0.25 g of ground sample was then weighed and slowly added to the mixture in the conical flask while agitating the flask to avoid agglomeration.
- The mixture was shaken in a mechanical shaker, for 30 min.
- The mixture was filtered through a vacuum filter using GF/C filter paper supported on a glass frit (before use the GF/C filter paper was dried at 105 °C and weighed).
- Care was taken to wash all residual material from the conical flask and also the walls of the funnel on to the filter.
- The residue on the filter paper was washed with deionised water seven times and three times with methanol.
- The filter paper was carefully removed and dried in an oven at 105 °C until a constant weight was achieved.

This method was followed for cement, and cement plus slag hydrated samples. In order to study the reliability of the selective

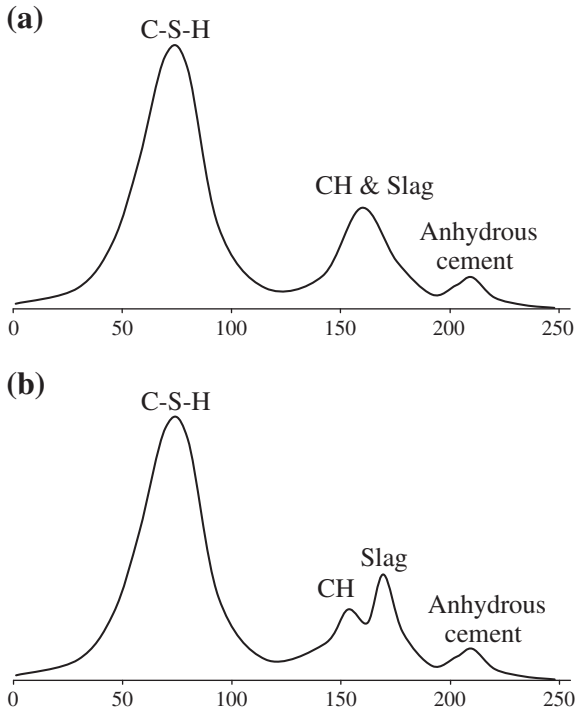

Fig. 2. Grey scale histograms showing the different components of Cement A–Slag 1 paste at 28 days (a) before and (b) after application of a median filter.

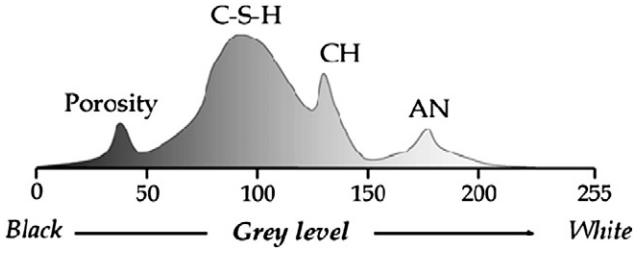

Fig. 1. Schematic grey level histogram for hydrated cement–slag paste at 20 °C.

dissolution, the residues were analysed by X-ray diffraction and examined by SEM.

3.4. Differential scanning calorimetry

Differential scanning calorimetry measurements were made with a Netzsch DSC/DTA Model 404 C Pegasus, using a 10 °C/min heating rate. The hydrated samples were ground, weighed (20 ± 4 mg) and placed in an alumina crucible pan, with an empty alumina crucible as a reference. A nitrogen flux was maintained in the heating chamber to avoid carbonation of the samples during the experiment.

3.5. Image analysis from BSE grey level images and EDS mappings from SEM

The polished sections were studied in backscattered electron (BSE) mode using a FEI quanta 200 SEM at an accelerating voltage of 15 kV.

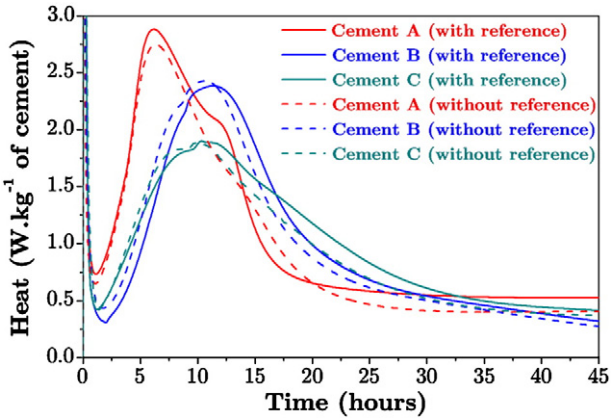

Fig. 4. Heat flow of 3 cements with different experimental conditions.

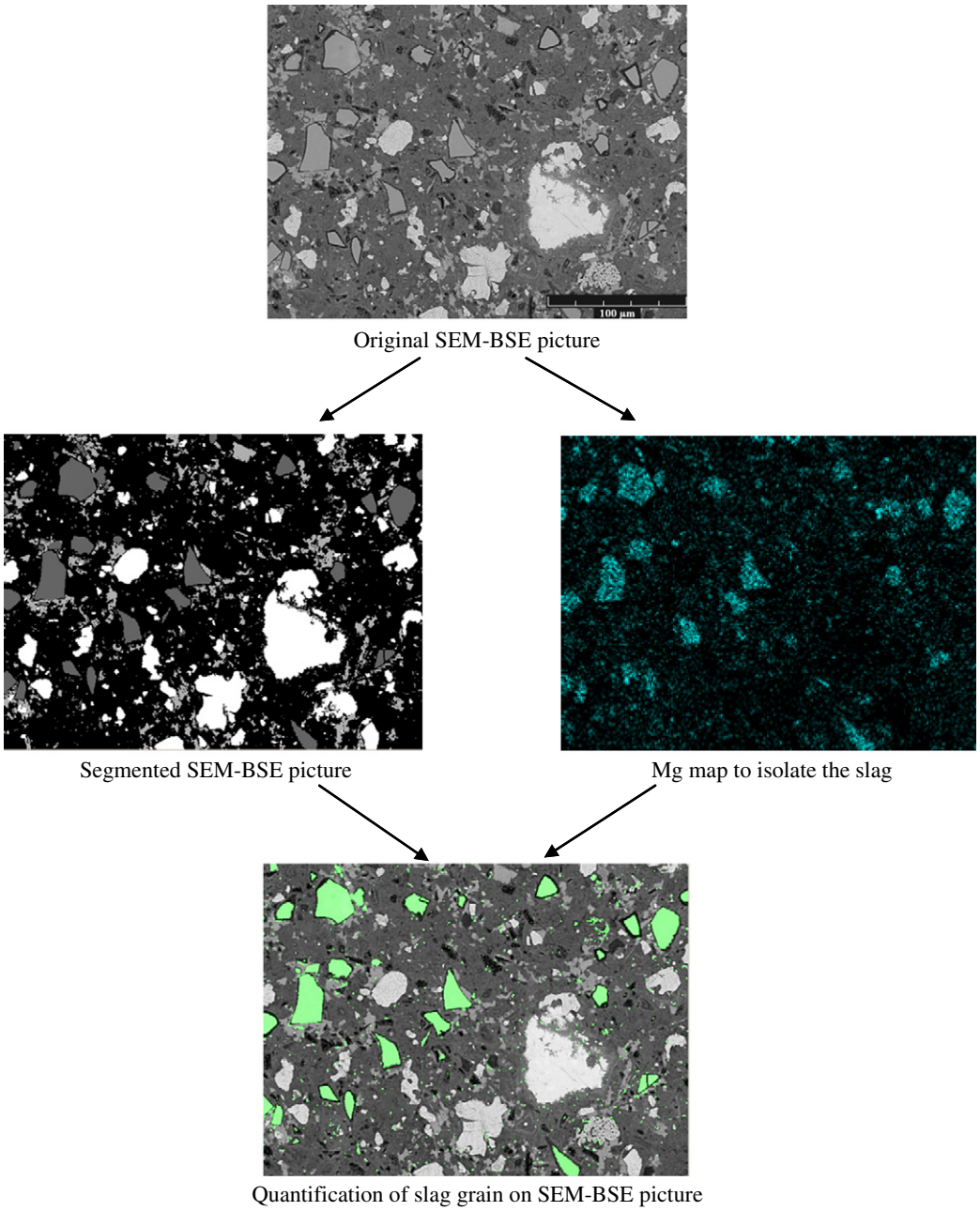

Fig. 3. BSE-image analysis combined with elemental mapping illustrated on example of Cement A–Slag 8 paste at 90 days.

Table 2
Undissolved materials and corresponding degree of reaction of slag after selective dissolution.

Label of samples	Undissolved materials (%)		Degree of reaction of slag (%)	
	Average	Standard deviation	Average	Standard deviation
Anhydrous S8	60.1	6.0	–	–
Anhydrous A-S8	67.5	5.7	–	–
Anhydrous B-S8	63.8	5.0	–	–
Anhydrous C-S8	61.9	5.9	–	–
A-S8 hydrated for 1 day	71.6	1.8	−79.0	4.4
B-S8 hydrated for 1 day	66.5	1.8	−66.3	4.6
C-S8 hydrated for 1 day	65.2	5.8	−63.1	14.6
A-S8 hydrated for 90 days	72.8	4.2	−82.0	10.5
B-S8 hydrated for 90 days	77.4	3.5	−93.5	8.8
C-S8 hydrated for 90 days	70.1	4.0	−75.1	9.9

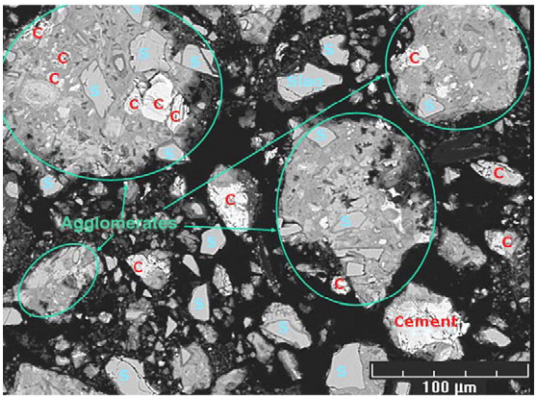

Fig. 6. BSE image of Cement B–Slag 8 hydrated 90 days after selective dissolution (C: Cement and S: Slag).

The phases were discriminated on the basis of the grey level histogram as shown in Fig. 1.

Slag 1 had a grey level sufficiently different from that of calcium hydroxide (CH) to allow its discrimination on the basis of the grey level only and after the application of a median filter, as illustrated in Fig. 2. A median filter replaces a pixel value by the median value of the pixels in the filter (3×3) and reduces the noise produced by imperfections in the image, while preserving strong contrast variations. On the other hand, Slag 8 had a composition and density which lead to a grey level matching exactly that of CH, which prevents the discrimination of the two phases on the basis of grey level segmentation. Therefore, in order to have a consistent methodology the slag in both systems was discriminated and segmented on the basis of their chemical signature using EDS chemical mappings of magnesium (significant levels of magnesium being present in the slag while not in CH) in addition to grey level as described below.

The challenge of this approach is the time to acquire Mg maps with a conventional EDS detector. To improve this, a silicon drift detector (SDD), type XFlash 4030 Detector from Bruker AXS Microanalysis was used which can accept a maximum input count rate of one million counts per second (cps). It also has a large active detecting area of 30 mm^2 (compared to 10 mm^2 for the conventional EDS detector) and at the same time achieves very good energy resolution of 133 eV (Mn Kα) at 100,000 cps. Even with this fast detector the time required to acquire 150–200 fields was about 10 h, but this was automated to run overnight.

For all blended systems, as illustrated in Fig. 3, the procedure consisted of:

- Acquisition of 150–200 BSE images (recorded in 30 s) combined with Mg maps (recorded in 1 min 30 s), at a nominal magnification of ×1000 (corresponding to 254×190 µm), at an accelerating voltage of 15 kV and a number of counts between 80,000 and 100,000 cps.
- Image analysis processing which combined the BSE image with the Mg map. The grains of unreacted slag were identified when the grey level of the pixel corresponded to the slag (from the BSE image) and contained Mg (from the EDS mapping image).
- Calculation of the degree of reaction according to Eq. (15).

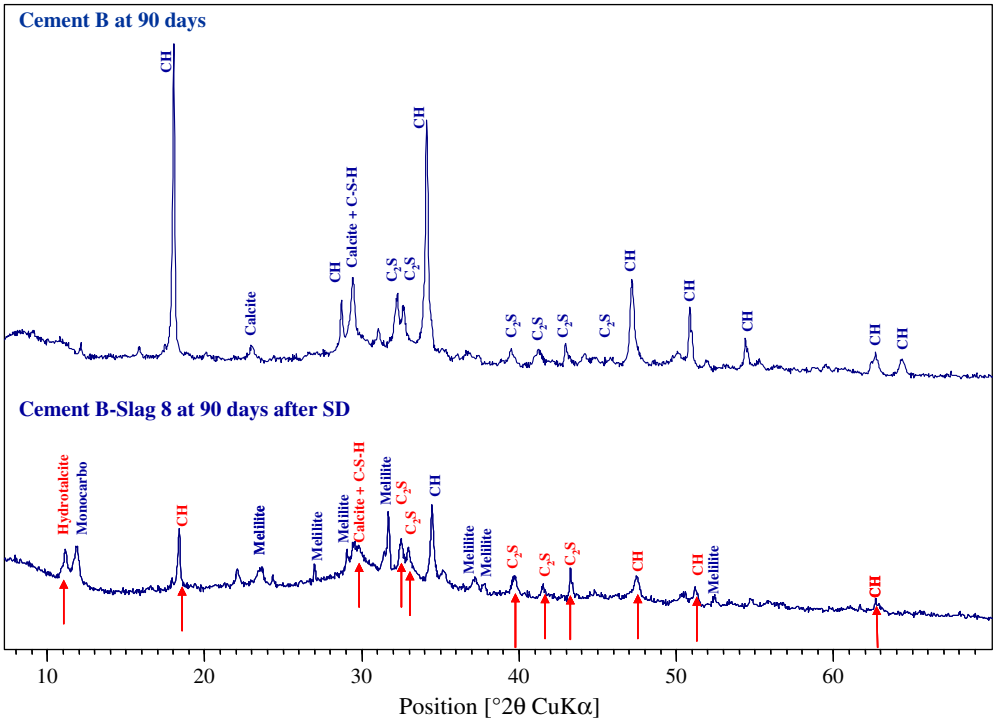

Fig. 5. XRD patterns of Cement B hydrated 90 days and Cement B–Slag 8 hydrated 90 days after selective dissolution.

Table 3
Results of analysis of residues after selective dissolution.

	100% dissolved phases	Partly dissolved phases	Non-dissolved phases
Anhydrous A-S8	C_3S, C_2S, C_3A, anhydrite	–	Slag 8
Anhydrous B-S8	C_2S, C_3A, C_4AF, anhydrite	C_3S	Slag 8
Anhydrous C-S8	C_2S, C_3A, anhydrite	C_3S	C_4AF, Slag 8
Hydrated A-S8	Ettringite	C_3S, C_2S, C–S–H, CH	Hydrotalcite, Slag 8
Hydrated B-S8	C_4AF, ettringite	C_3S, C_2S, C–S–H, CH	Hydrotalcite, Slag 8
Hydrated C-S8	C_4AF, ettringite	C_3S, C_2S, C–S–H, CH	Hydrotalcite, Slag 8

3.6. Isothermal calorimetry

The heat of reaction of the pastes at 20 °C was measured with an isothermal calorimeter (TAM Air from TA instruments). It consists of 8 parallel twin measurement channels maintained at a constant temperature: one from the sample, the other for the reference sample.

Preliminary work [44] underlined that it is critical to balance the specific heats of the sample and reference, particularly for measurements over the long time periods used here, where the rate of heat evolution becomes very low. In this work, the reference was deionised water calculated to have the same specific heat as the paste [45]:

$$C_p^{\text{paste}} = x^{\text{water}} C_p^{\text{water}} + x^{\text{cement}} C_p^{\text{cement}} \quad (11)$$

Where:

x^{water}: mass fraction of water in paste;
x^{cement}: mass fraction of cement in paste;
C_p^{water}: specific heat of water;
C_p^{cement}: specific heat of cement.

Considering, the water-cement ratio of 0.4, $C_p^{\text{water}} = 4.18\ J.g^{-1}.K^{-1}$ [46] and $C_p^{\text{cement}} = 0.75\ J.g^{-1}.K^{-1}$ (based on the measured values for tricalcium silicate and dicalcium silicate [47]) we found a specific heat of cement paste of $1.73\ J.g^{-1}.K^{-1}$. The optimal quantity of paste was 15 g with a 6.2 g glass ampoule of water as a reference.

The thermal inertia is expressed by the time constant of a calorimeter which depends on two parameters: the sample heat capacity and the heat transfer properties of the calorimeter. The measured time constant has been used to correct the output signal (Tian correction) for the thermal inertia of the calorimeter especially at very early ages as shown below:

$$P(t) = \varepsilon\left(U + \tau\frac{dU}{dt}\right) \quad (12)$$

With:

$P(t)$: the thermal power produced in the sample (Watts);
U: the voltage output of the heat flow sensors (Volts);
ε: the calibration factor (W/V);
τ: the time constant of the calorimeter (s) which has been calculated to be 4 min.

Fig. 4 shows the importance of correct calibration and choice of reference sample to the rate of heat evolution curves. Although the general shapes of the peaks are similar, the absolute values vary, which can lead to substantial errors when the total heat evolution is calculated by integration over long times.

3.7. Chemical shrinkage

The chemical shrinkage setup was designed and optimised at EPFL [43] and it consists of a cylindrical flask (2 cm height by 1 cm of diameter) that contains the paste, on top of which a pipette is connected. The level of paste introduced in the flask was kept constant in all measurements and equal to 1 cm (5 g of paste). The paste was tapped in order avoid the presence of entrapped bubbles. Water was added immediately to the top of the paste, taking special care to avoid as much as possible the dilution of the paste.

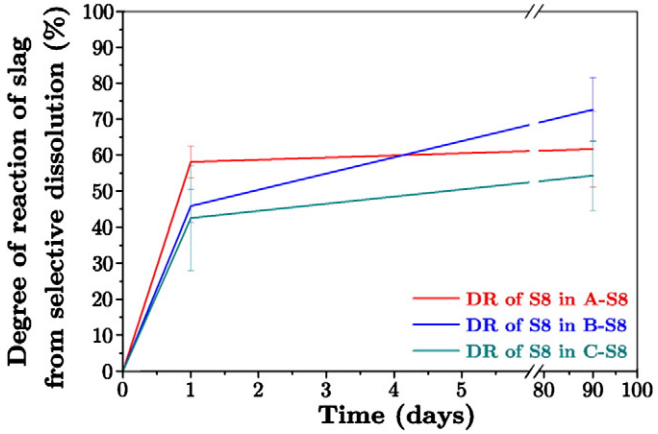

Fig. 7. Degree of reaction of slag from selective dissolution after corrections suggested in [17].

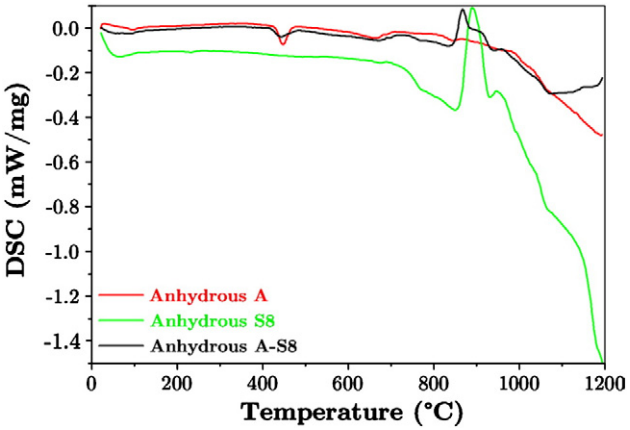

Fig. 8. DSC curves of anhydrous powders.

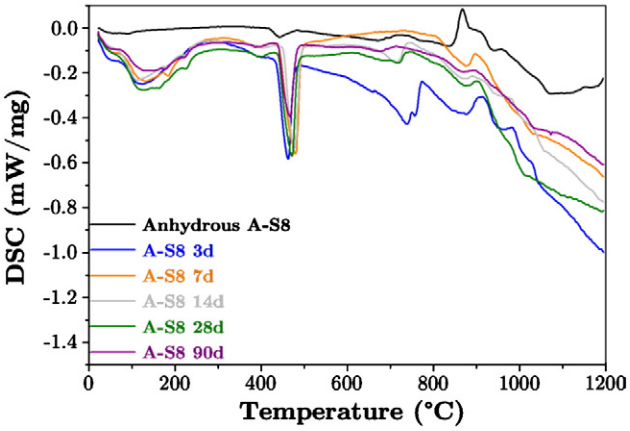

Fig. 9. DSC curves of Cement A blended with Slag 8 at different ages.

Water is added on top of the cement paste until it fills also the pipette. The system is sealed at the interface between the pipette and the flask with rubber lids and on top of the pipette with a coloured oil drop. This coloured oil drop is used as a tracer in the image analysis of the pictures of the capillary taken with a webcam. The flasks are maintained in a thermostatic bath at 20 °C to avoid effects of heat release on volumetric changes of the paste.

As the hydration proceeds and the paste shrinks, the level of water in the pipette decreases. This level is monitored using a webcam connected to a computer that allows automated acquisition every 5 min. To extract the level of water in the pipette, the pictures were numerically processed. Each curve presented is the average of a minimum of 3, but mostly 6, replicates of a cement paste system.

4. Results and discussion

4.1. Selective dissolution

Considering that the selective dissolution does dissolve the unhydrated cement grains and their hydration products, leaving only the

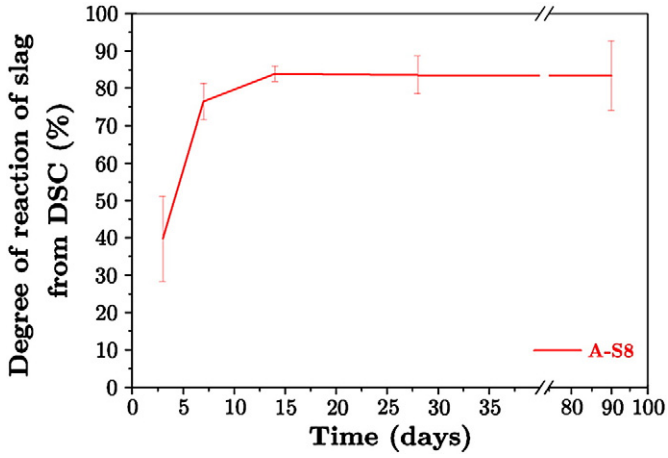

Fig. 11. Apparent degree of reaction of Slag 8 from DSC in Cement A–Slag 8 blended pastes.

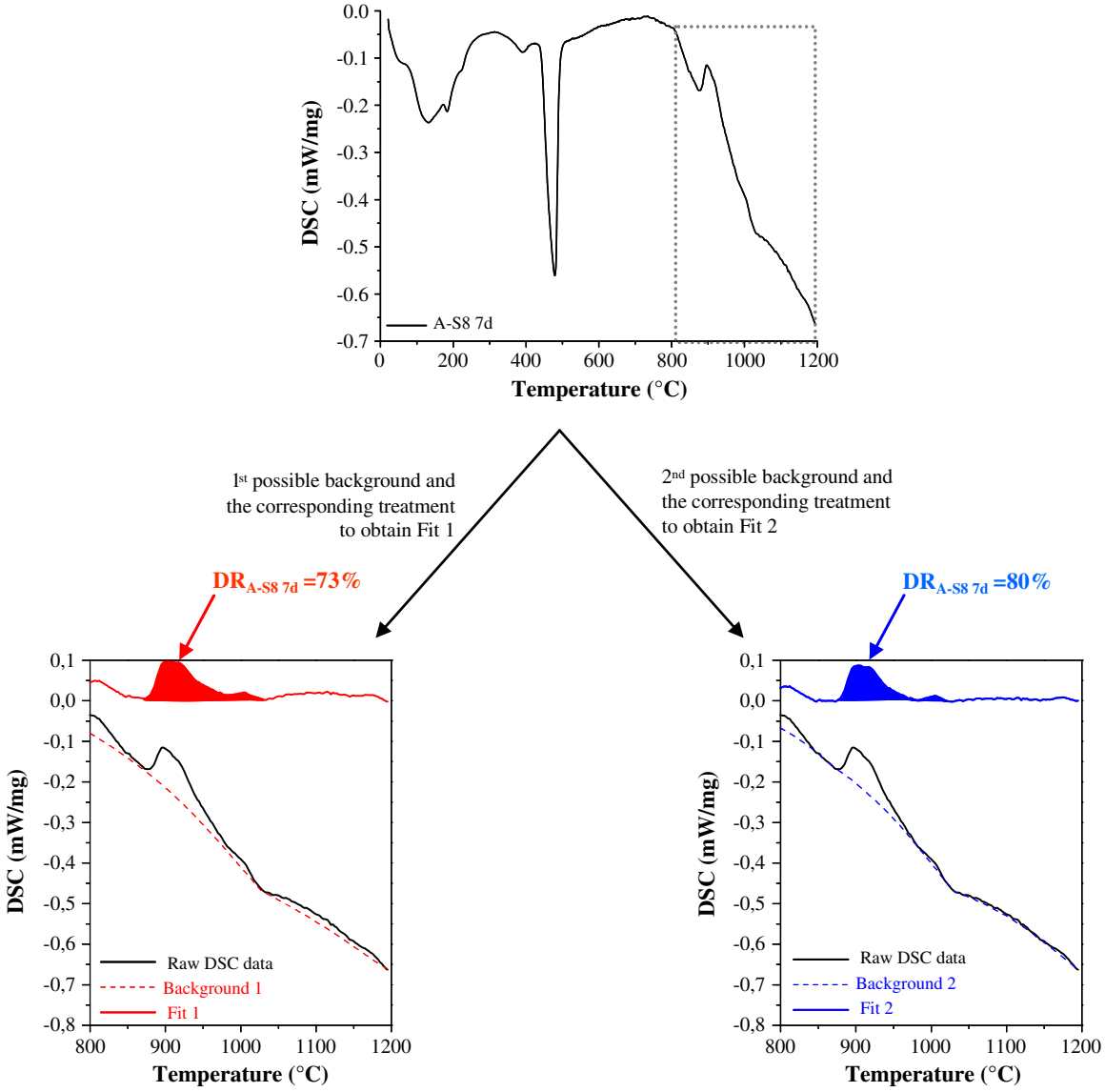

Fig. 10. Method for background removal algorithm on DSC curve of Cement A–Slag 8 hydrated 7 days.

unreacted slag grains as undissolved residue, the degree of hydration of slag grains in pastes can be calculated from Eq. (13):

$$\alpha_{SLAG}^{Selectivedissolution} = \frac{R_{cement} - R_{paste}}{R_{cement}} \quad (13)$$

Where:

R_{cement}: undissolved residue from the blended anhydrous cement;
R_{paste}: undissolved residue from the cement paste.

Table 2 shows the percentage of non-dissolved materials and the supposed degree of reaction of slag for the hydrated mixes. From the data it is evident that the undissolved materials (expressed as a percentage of the total amount), do not correspond only to the unreacted slag because the percentage is much higher than the initial content of the slag (40%wt), which would imply a negative degree of reaction.

In order to study the reliability of the selective dissolution, the residues were examined by XRD and SEM. The residues showed undissolved phases (other than slag) in both the anhydrous blends and hydrated samples. Fig. 5 shows XRD patterns of Cement B hydrated for 90 days and Cement B–Slag 8 hydrated 90 days after selective dissolution. The pattern of Cement B clearly shows the presence of phases from the cement that selective dissolution should remove in the blended pastes: notably belite and portlandite. The pattern from the blended paste also indicates the presence of hydrotalcite from the hydration of slag and which should also be removed by the selective dissolution. Fig. 6 shows the residue from the selective dissolution of Cement B–Slag 8 hydrated 90 days, embedded in resin and polished for examination by SEM-BSE, this clearly shows the presence of undissolved cement grains, hydrated phases and agglomerates.

The characterisation of the different phases in the selective dissolution residues by XRD analysis and SEM is summarised in Table 3. For the anhydrous blends, selective dissolution did not completely dissolve the clinker phases for Cements B and C. Dissolution was better for Cement A probably due to its higher fineness compared to Cements B and C. For the hydrated mixes, only ettringite and ferrite were 100% dissolved, the other anhydrous and hydrated phases

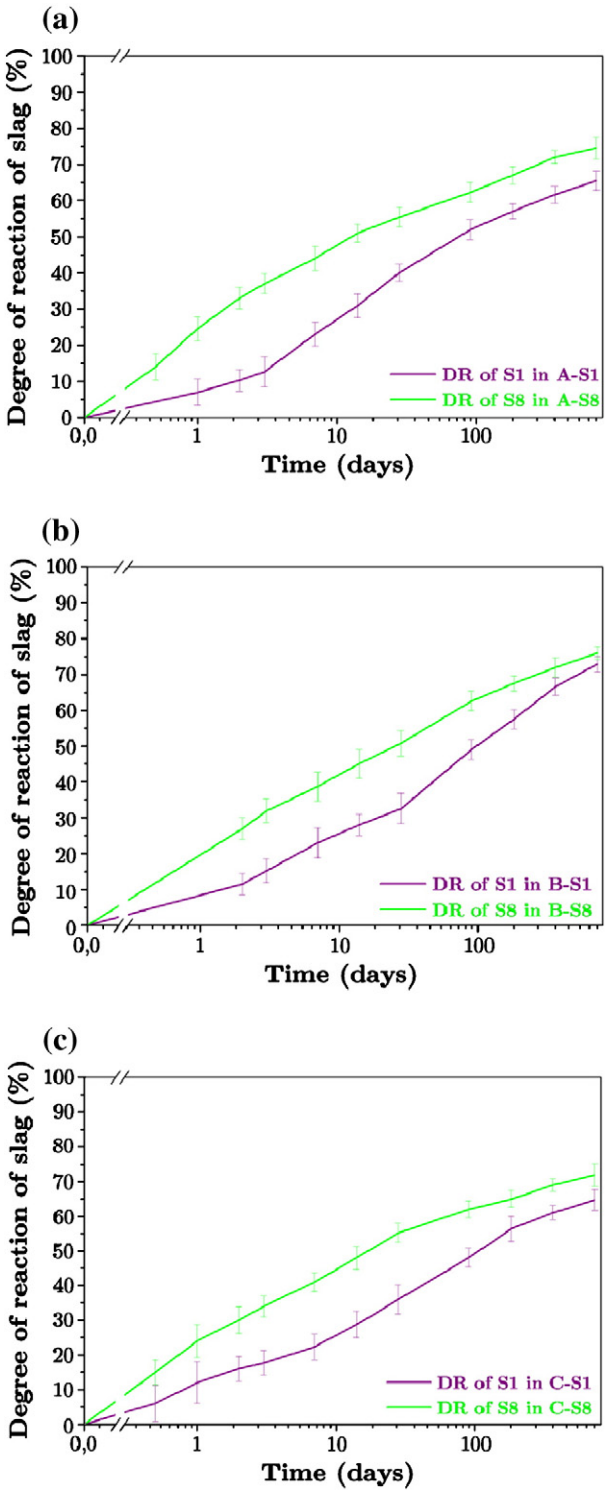

Fig. 12. Degree of reaction of slag from SEM-BSE-IA-mapping in (a) systems A, (b) systems B and (c) systems C.

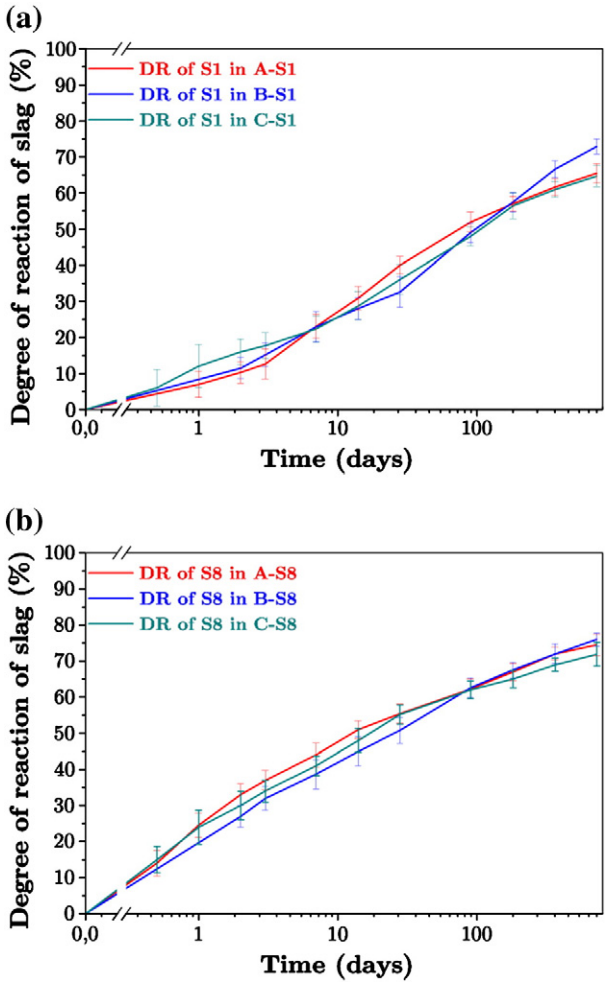

Fig. 13. Degree of reaction of (a) Slag 1 and (b) Slag 8 from SEM-BSE-IA-mapping in blended pastes.

were not completely dissolved and hydrotalcite was also observed in the residues by XRD.

Since the sample mass of 0.25 g appeared very small, measurements were repeated adapting the procedure with higher masses (0.5 g, 1.0 g and 1.5 g) and some tests with smaller filtration system were also conducted. These modifications made no significant difference to the results.

Some authors [17] have proposed a modification to recalculate the degree of reaction of slag with the following formula:

$$\alpha_{SLAG}^{Selectivedissolution}(t) = 100 - \left(\frac{w_2 + (\%_{SLAG}(t=0)\%_{DISSOLVEDSLAG}\, w_1) - (\%_{CEMENT}(t=0)C_r w_1)}{\%_{SLAG}(t=0)w_1}100\right) \quad (14)$$

Where:

w_1: weight of sample (ignited weight);
w_2: weight of residue (105 °C dry weight);
C_r: percentage of residue from cement divided by 100;
$\%_{SLAG}(t=0)$: percentage of initial slag in the blended cement (equal to 40%);
$\%_{CEMENT}(t=0)$: percentage of initial cement in the blended cement (equal to 60%).
$\%_{DISSOLVED\ SLAG}$: assumption of 6% of slag dissolves.

This approach gives the results shown in Fig. 7. Although the degrees of reaction are now positive, they are very high, especially at 1 day.

It might be argued that further work, for example, on optimising the grinding process could have led to better results for the selective dissolutions method. However, this underlines the problem of the reproducibility of the method betweens labs. In a recent study of selective dissolution methods for fly ash, Ben Haha et al. [48] noted the different assumptions needed to calculate the amount of reaction are a major cause of errors, which renders such methods inadequate for quantifying the degree of reaction. It is also clear from the literature that very divergent results are reported for this method by different workers studying nominally similar slags: For example, Escalante et al. [20] find degrees of reaction of about 20% after 3 months compared to values of around 40% reported by Luke and Glasser [17] and Lumley et al. [19].

In the light of the current results and the diversity of results in the literature, we consider, that; while such methods could be suitable to enrich materials with respect to certain phases for other characterisation methods such as NMR [28,49], they are not reliable for the quantitative determination of the degree of reaction.

4.2. Differential scanning calorimetry

Fig. 8 shows the DSC curves of three anhydrous powders: pure Cement A, pure Slag 8 and the A-S8 blended powder. For the raw slag and the blended powder, the recrystallisation peaks of slag can be identified between 850 and 1050 °C. The objective was to isolate and measure the recrystallisation peak in order to quantify the degree of reaction of slag. The experiments were conducted on one blended system (Cement A–Slag 8). The DSC curves at various hydration times (Fig. 9) show that the recrystallisation peak decreases with time, but there is also a strong change in the background. The large contribution of the background was already noted in previous DSC analyses on plain OPC [50].

To remove the contribution of the background, a manual method with the DSC software was judged too subjective. So a background removal algorithm was applied with two different choices of reasonable backgrounds which led to two different degrees of reaction of slag for each analysed sample. An example of the method is shown in Fig. 10 and the results are shown in Fig. 11. As for results from selective dissolution, it is seen that there is an unreasonably high degree of hydration at 7 days and little evolution in time thereafter. It was concluded that the DSC method was unreliable due to the large error produced by the background.

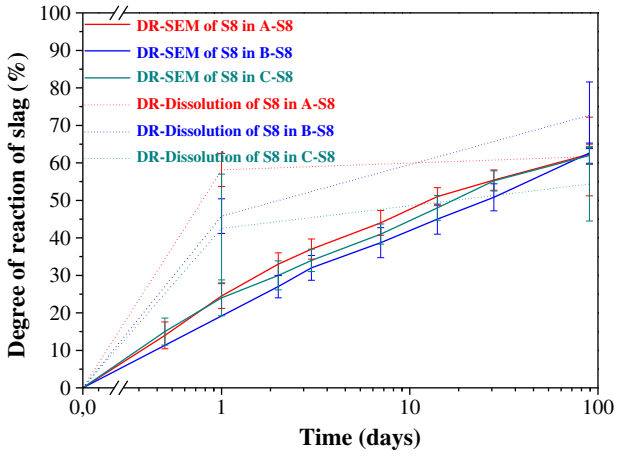

Fig. 14. Degree of reaction of Slag 8 from selective dissolution and SEM-BSE-IA-mapping.

4.3. Image analysis from BSE grey level images and EDS mappings from SEM

Assuming the original volume of the slag in the paste, the degree of reaction of slag can be estimated by image analysis of the area fraction (equivalent to volume fraction) remaining at a given time:

$$\alpha_{SLAG}^{SEM\text{-}IA}(t) = \frac{Vf_{anhydrousslag}(t=0) - Vf_{anhydrousslag}(t)}{Vf_{anhydrousslag}(t=0)} \quad (15)$$

Where:

$Vf_{anhydrous\ slag}(t=0)$: remaining volume fraction of initial anhydrous slag;
$Vf_{anhydrous\ slag}(t)$: remaining volume fraction of unreacted slag after time t.

Fig. 12 shows the degree of reaction of slag for all the systems as a function of type of cement. With the fast EDS detector it was possible to obtain results with reasonable precision; the errors indicated in Fig. 12 take into account the deviation between different sets of images from the same sample and the deviation from different possible treatments to define the border of slag grain. The errors are higher at

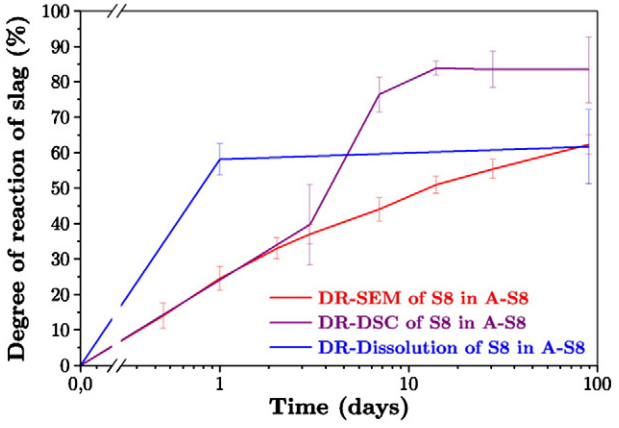

Fig. 15. Degree of reaction of Slag 8 from SEM-BSE-IA-mapping, DSC and selective dissolution.

early ages. The results clearly show that Slag 8 is more reactive than Slag 1. Fig. 13 shows the degree of reaction of slag for each slag for the different cements. It seems that the reaction of slag is not strongly affected by type of cement.

The results from SEM-BSE-IA-mapping are compared to the ones from selective dissolution and DSC in Figs. 14 and 15. These indicate that selective dissolution and DSC significantly overestimate the degree of reaction of slag at early ages.

Despite being a time consuming method, the determination of the degree of reaction of slag using SEM with image analysis and elemental mapping treatment appears to be the most reliable of the methods based on analyses of the systems as discrete time intervals.

4.4. Isothermal calorimetry

Fig. 16 shows the cumulative heat evolution curves, normalised to clinker content, of pastes blended with Cement B over a period of 28 days. The heat evolved from the blended pastes (normalised per gram of cement (i.e. ground clinker plus calcium sulfate component)) rapidly surpasses that of the 100% cement paste. This difference includes both the contribution from the reaction of the slag itself and the impact of the physical presence of slag on the rate of hydration of the clinker phases, *filler effect*. The filler effect consists of two possible elements. As the filler does not react, the space available for the hydrates of the clinker is increased which leads to a higher degree of reaction of the cement. For fillers with high surface area there may be an additional effect of stimulating nucleation. To separate these effects, a blend with 40% quartz (presumed inert) was used as another reference. The quartz was ground to have a similar particle size range as the slag (d_{50} of filler = 10 μm and d_{50} of Slag 1 = 20 μm and d_{50} of Slag 8 = 15 μm). For each cementitious system, all calorimetry experiments were run in concurrently over 28 days. To insure a good accuracy of the results and to verify the

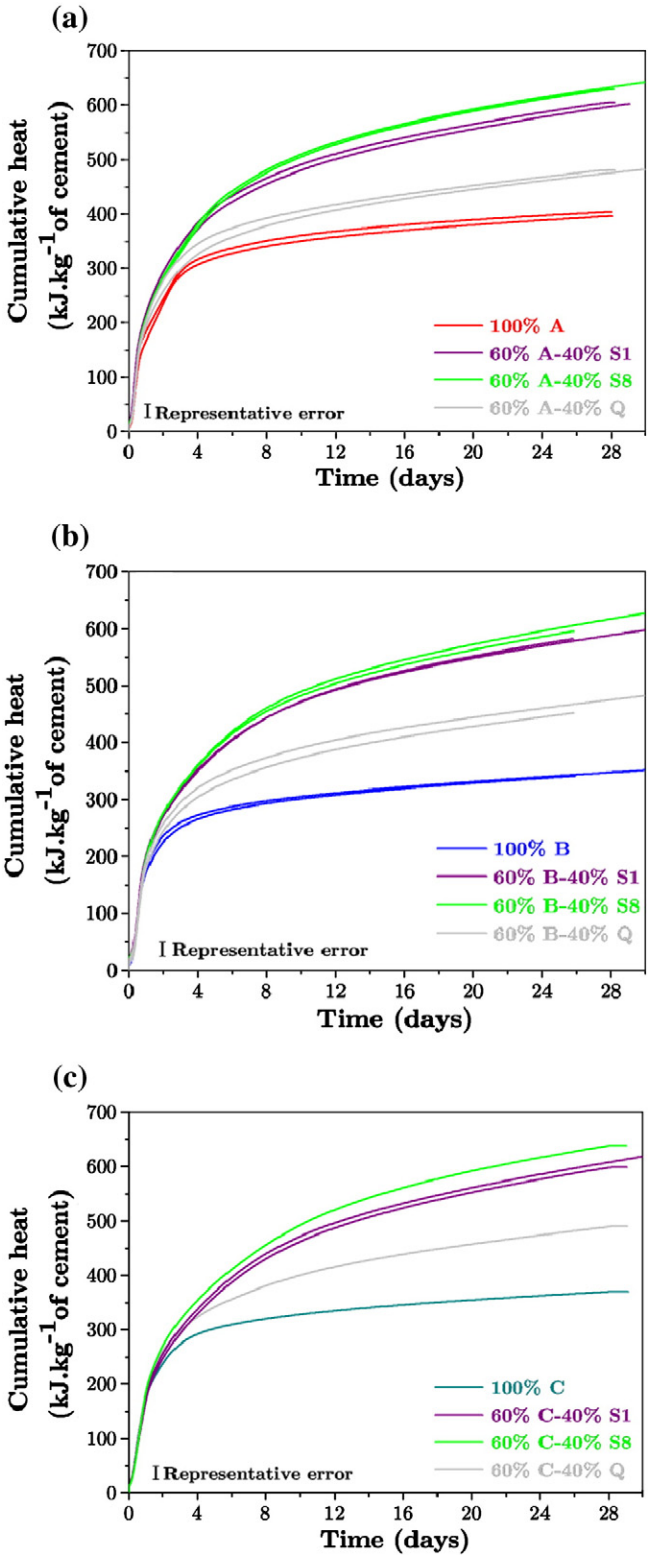

Fig. 16. Normalised cumulative heat curves for (a) systems A, (b) systems B and (c) systems C.

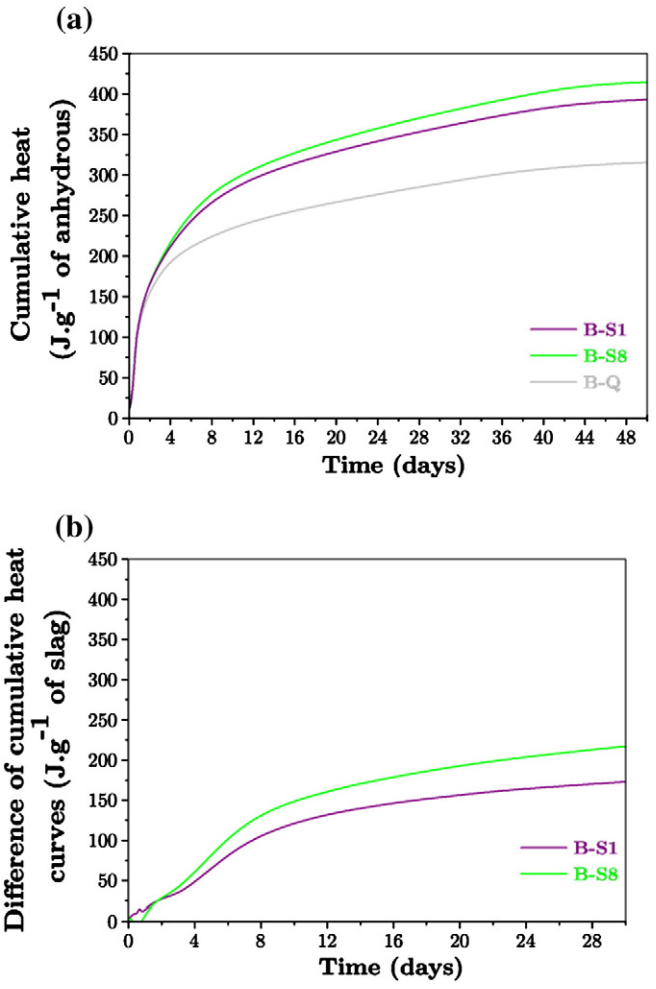

Fig. 17. (a) Cumulative heat per gram of anhydrous and (b) resulting difference curves which isolate the slag contribution.

stability of the baseline, all the experiments were repeated twice. Fig. 16 shows that the repeatability between different batches was good even for long term acquisition.

The divergence of the curves from the filler reference is attributed to the reaction of the slag itself. In agreement with the image analysis results Slag 8 is clearly more reactive than Slag 1. In order to quantify the contribution of slag the curve of the blend with quartz is subtracted from that of the blend with slag and then normalised by the amount of slag, Fig. 17. However the resulting curve of $J.g^{-1}$ of slag cannot be directly related to a degree of reaction as we do not know the heat evolved by the reaction of a unit weight of slag. A value of 460 $J.g^{-1}$ of slag can be found in the literature [51], but, it seems [52] this was derived from the adiabatic heat rise in the first day, when the degree of reaction of slag is negligible and in fact describes the filler effect of slag on the hydration of cement. Some old papers [53,54] suggest to use of the solubilities of hydroxides which form hydrates of slag to calculate the enthalpy of slag, but the values obtained by this method were too high to be reasonable.

To obtain calibration values for the enthalpy of slags, the difference curve from calorimetry was compared to the values of degree of reaction from image analysis (Fig. 18). Given the larger error in the BSE-IA results at early ages the curves were calibrated from the values at 28 days giving the values shown in Table 4. Although one may expect the calibration factors to be the same for the same slag with different cements higher values are found for systems B with Cement B and Slag 1. The reasons for this discrepancy are not yet understood.

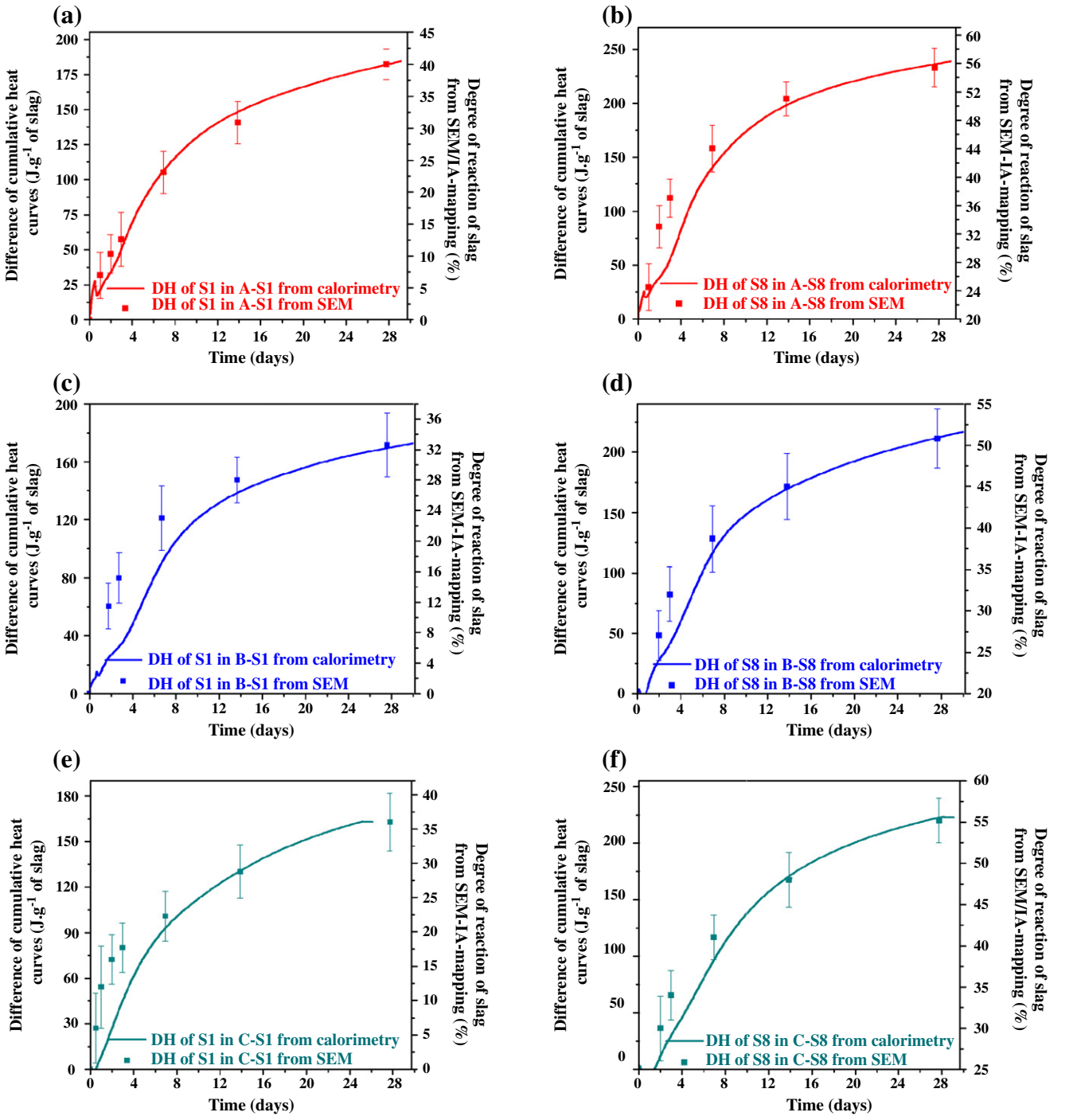

Fig. 18. Calorimetry curves calibrated with SEM-BSE-IA-mapping in (a) systems A-S1, (b) systems A-S8, (c) systems B-S1, (d) systems B-S8, (e) systems C-S1 and (f) systems C-S8.

Table 4
Calibration factor to correlate difference of cumulative curves from calorimetry with degree of reaction of slag from SEM-BSE-IA-mapping.

	Degree of reaction of slag from SEM-BSE-IA-mapping	Cumulative heat ($J.g^{-1}$ of slag)	Calibration factor ($J.g^{-1}$ of slag)
A-S1 at 28 days	0.418 ± 0.008	182 ± 10	436 ± 32
B-S1 at 28 days	0.326 ± 0.014	170 ± 10	521 ± 53
C-S1 at 28 days	0.375 ± 0.014	165 ± 10	440 ± 43
A-S8 at 28 days	0.554 ± 0.009	237 ± 10	428 ± 25
B-S8 at 28 days	0.508 ± 0.012	213 ± 10	419 ± 30
C-S8 at 28 days	0.552 ± 0.009	223 ± 10	404 ± 25

4.5. Chemical shrinkage

For chemical shrinkage, an approach analogous to that described for calorimetry was used. For each system, the curve of filler was subtracted from the blended one to isolate the contribution of the slag. Fig. 19 shows a good repeatability between two different batches. Here again, the curves indicate the higher reactivity of Slag 8 compared to Slag 1 in all blended pastes. The plot of calorimetry versus chemical shrinkage shows a linear relation for pure and blended pastes, Fig. 21. This indicates no major change in the nature of reaction or density of hydration products for the plain and blended systems.

As explained above for calorimetry, an independent calibration of each chemical shrinkage curve was made using the degree of reaction of the slag from SEM-BSE-IA-mapping (Fig. 20). The calibration factors used the 28 days as the reference values (see Table 5). As previously found for calorimetry, the calibration factor is higher for system B-S1.

5. Conclusions and discussion

A number of methods were studied to determine the amount of slag reacted in hydrated blended systems. Two of these methods — selective dissolution and thermal analysis, did not give reasonable results in this study.

The results presented indicate that the most promising methods to study the degree of reaction of the slag are image analysis and isothermal calorimetry or chemical shrinkage.

By image analysis the degree of reaction can be measured directly from the amount of unhydrated slag remaining. However this method has some limitations:

- First it is rather time consuming, the essential prerequisite is a well polished sample, this takes 5 h and due to the differential hardness of the slag it is especially difficult to obtain good sample preparation at young ages (up to one day).
- Second the differentiation of the slag grey level alone is not reliable for some compositions, due to the close similarity of the grey levels of slag and calcium hydroxide. For some slag compositions, the use of appropriate filters can differentiate these two phases, but nevertheless these image processing steps will mean that very small particles are not well measured, which increases the error at young ages. For other compositions the BSE images must be combined with Mg maps to isolate the slag, which requires an image acquisition time of around 10 h (although this process can be automated and carried out overnight). In both cases, the low amount of slag remaining leads also to relatively low precision in the degree of hydration.

Isothermal calorimetry, if performed in a well calibrated and stable instrument is a potentially powerful method to measure degree of reaction. The technique provides continuous and precise values, but is difficult to calibrate. Calibration against the image analysis results was done in this study and some results seem anomalous, so clearly more work is needed on a wider range of materials.

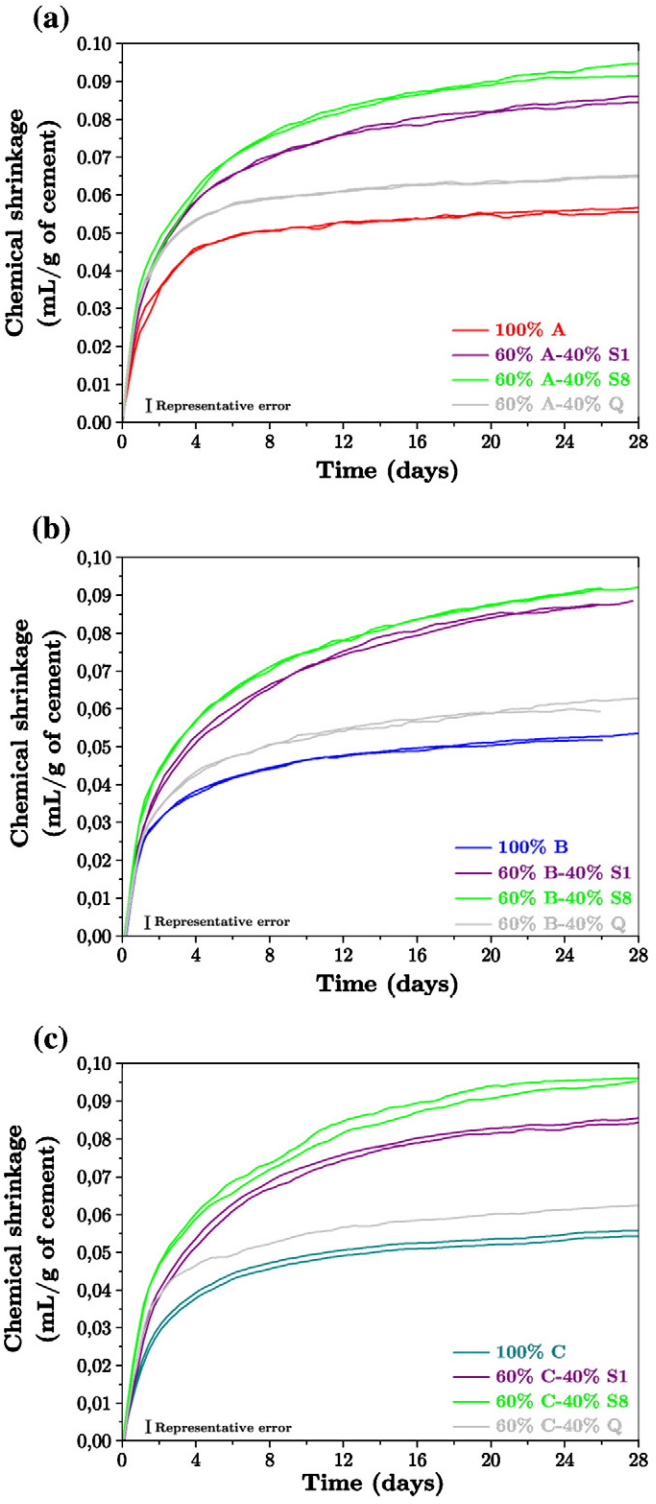

Fig. 19. Evolution of chemical shrinkage for (a) systems A, (b) systems B and (c) systems C.

Chemical shrinkage measurements give results analogous to isothermal calorimetry. Using the methodology described here, this is by far the least expensive method.

Table 6 summarises the main parameters in different methods. The validity of our quantification of slag reaction was verified using comparison with results from NMR given by Poulsen [55,56]. It is very difficult to determine the degree of hydration for slags directly from the ^{29}Si MAS NMR spectra due to severe overlap of the slag peak with the resonances from alite, belite, and the C–S–H phase

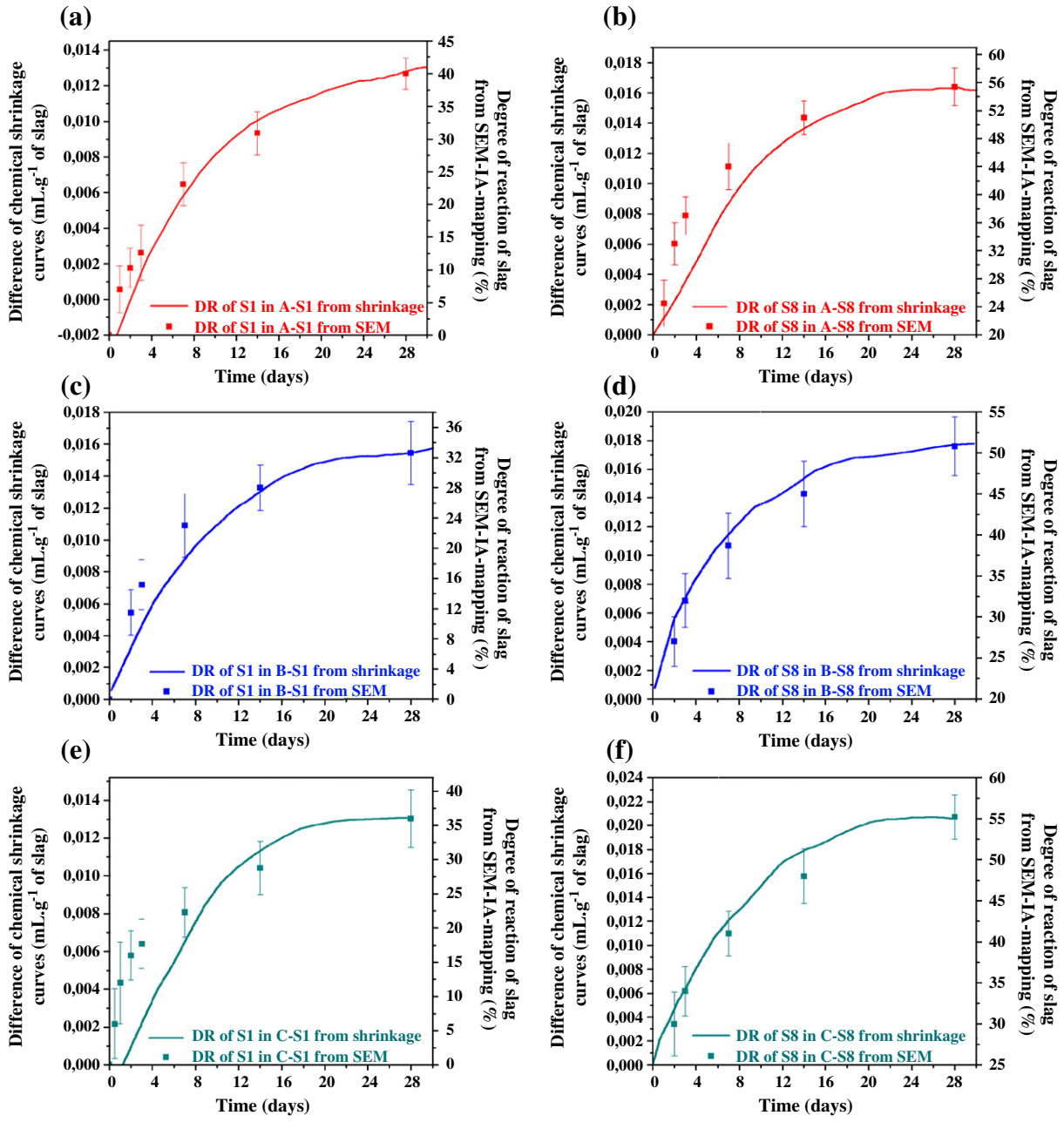

Fig. 20. Chemical shrinkage calibrated with SEM-BSE-IA-mapping for (a) systems A-S1, (b) systems A-S8, (c) systems B-S1, (d) systems B-S8, (e) systems C-S1 and (f) systems C-S8.

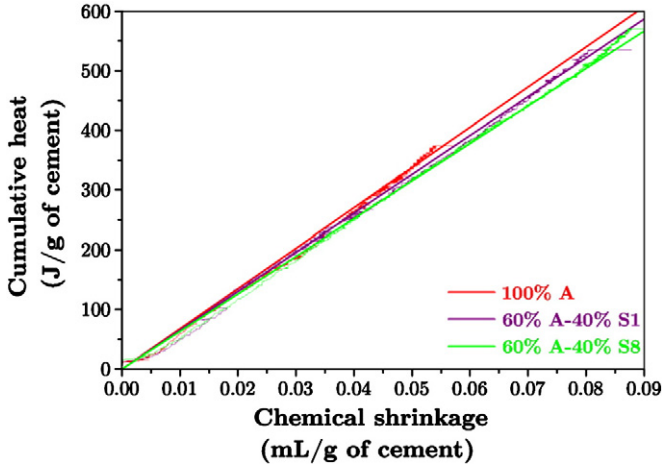

Fig. 21. Calorimetry versus chemical shrinkage results for systems A.

of the hydrating cement. Therefore, a new method based on ^{27}Al MAS NMR was used to obtain quantitative estimates for the degree of slag hydration.

Fig. 22 shows that the results from NMR are a bit lower than the ones from SEM-BSE-IA-mapping for systems A-S1 and C-S8. However, for

Table 5
Calibration factor to correlate difference of chemical shrinkage curves with degree of reaction of slag from SEM-BSE-IA-mapping.

	Degree of reaction of slag from SEM-BSE-IA-mapping	Chemical shrinkage (mL.g^{-1} of slag)	Calibration factor (mL.g^{-1} of slag)
A-S1 at 28 days	0.418 ± 0.008	0.0128 ± 0.0025	3.1E−02 ± 6.6E−03
B-S1 at 28 days	0.326 ± 0.014	0.0154 ± 0.0025	4.7E−02 ± 9.7E−03
C-S1 at 28 days	0.375 ± 0.014	0.0131 ± 0.0025	3.5E−02 ± 8.0E−03
A-S8 at 28 days	0.554 ± 0.009	0.0163 ± 0.0025	2.9E−02 ± 5.0E−03
B-S8 at 28 days	0.508 ± 0.012	0.0177 ± 0.0025	3.5E−02 ± 5.7E−03
C-S8 at 28 days	0.552 ± 0.009	0.0206 ± 0.0025	3.7E−02 ± 5.1E−03

Table 6
Comparison between different methods used to calculate the degree of reaction of slag.

Method	Type of measurement	Time of acquisition per sample	Time to treat the results	Comments
Selective dissolution	Discrete	20 min	5 min	Remaining undissolved phases which induced large errors on the degree of reaction of slag
DSC	Discrete	2 h	20 min	Overlap between peak of belite and the one of slag which does not allow to isolate the slag contribution
SEM-BSE-Image analysis-mapping	Discrete	10 h	1 h	Good accuracy but time consuming
Calorimetry	Continuous		1 h	Needs to be calibrated with an external method
Chemical shrinkage	Continuous		1 h	Needs to be calibrated with an external method

system A-S8, there was a good agreement with SEM-BSE-IA-mapping results. At present the errors for the NMR method are not well established. However, the NMR results also clearly show that the Slag 8 was more reactive than Slag 1 and confirm that the values obtained by selective dissolution and DTA at early ages are over estimates.

All our investigations indicated that Slag 8 (high alumina and alkali contents) had a higher reactivity than Slag 1 (high amorphous content). This difference in reactivity was confirmed for reaction of slag

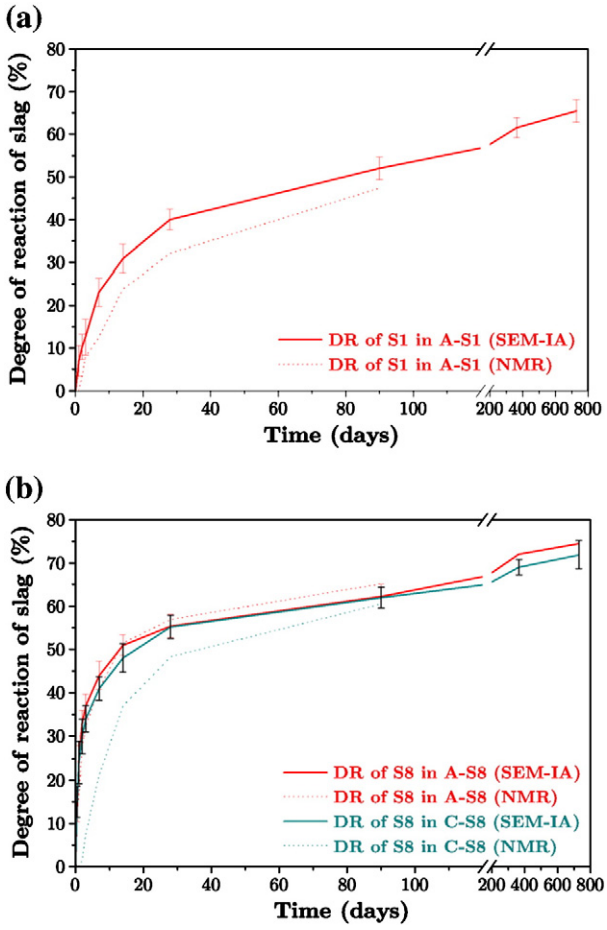

Fig. 22. Comparison of degree of reaction of (a) Slag 1 and (b) Slag 8 from NMR and SEM-BSE-IA-mapping.

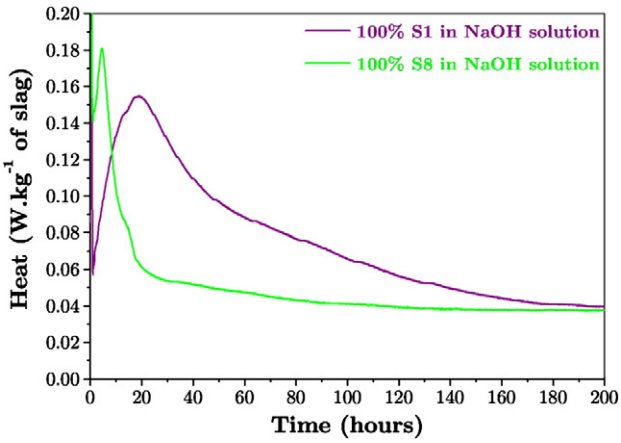

Fig. 23. Heat curves of both slags activated by NaOH solution.

in pure NaOH solution as shown by the calorimetry results for such systems in Fig. 23. Slag 8 is quickly and strongly dissolved in NaOH solution comparing to Slag 1 which reacts more slowly.

The relative rate of reaction of Slag 8 and Slag 1 can be compared with different reactivity indices. For example, Fig. 24 plots M1 = CaO/SiO_2 and M5 = $(CaO + MgO + Al_2O_3)/SiO_2$ against degree of reaction of slag from SEM. These reactivity indices rank the two slags differently, and while the ranking given by the M5 index corresponds to the ranking of reactivity by image analysis it is not possible to draw further conclusions based on the study of only two slags.

Comparison of the effects of using low and high alkali cement (respectively Cements C and B) in combination with slag did not indicate any significant difference in reaction rate at early ages. In this work, it was observed that the differences in cement clinker had very little impact on the reaction of the slags.

Acknowledgments

The authors thank the NANOCEM consortium for funding this study. Dr Shashank Bishnoi is thanked for the program to process the chemical shrinkage data. Dr Cyrille Dunant is thanked for his contribution to establish the background removal algorithm to treat the DSC curves. Dr Patrick Juilland is thanked for his help to perform the calibration and the stability of the calorimeter. Dr Søren Poulsen and Professor Jørgen Skibsted are thanked for their results on degree of reaction of slag obtained by NMR.

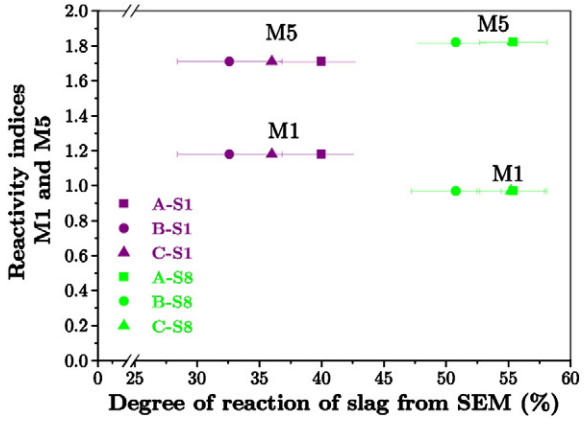

Fig. 24. Reactivity indices M1 and M5 versus degree of reaction of slag from SEM-BSE-IA-mapping.

References

[1] I. Pane, W. Hansen, Investigation of blended cement hydration by isothermal calorimetry and thermal analysis, Cem. Concr. Res. 35 (6) (2005) 1155–1164.
[2] B.K. Marsh, R.L. Day, Pozzolanic and cementitious reactions of fly ash in blended cement pastes, Cem. Concr. Res. 18 (2) (1988) 301–310.
[3] M. Mouret, A. Bascoul, G. Escadeillas, Study of the degree of hydration of concrete by means of image analysis and chemically bound water, Adv. Cem. Based Mater. 6 (3–4) (1997) 109–115.
[4] Zhang X., Quantitative microstructural characterisation of concrete cured under realistic temperature conditions, PhD thesis, Ecole Polytechnique Fédérale de Lausanne, 2007.
[5] Gallucci E., Zhang X. and Scrivener K.L., Effect of temperature on the microstructure of calcium silicate hydrate (C–S–H), Cement and Concrete Research, submitted for publication
[6] K.L. Scrivener, Backscattered electron imaging of cementitious microstructures: understanding and quantification, Cem. Concr. Compos. 26 (8) (2004) 935–945.
[7] J.C. Taylor, L.P. Aldridge, C.E. Matulis, I. Hinczak, Chapter 18: X-ray powder diffraction analysis of cements, in: J.B.P. Barnes (Ed.), Structure and Performance of Cements, Spon Press, 2001, pp. 420–441.
[8] K.L. Scrivener, T. Fullmann, E. Gallucci, G. Walenta, E. Bermejo, Quantitative study of Portland cement hydration by X-ray diffraction/Rietveld analysis and independent methods, Cem. Concr. Res. 34 (9) (2004) 1541–1547.
[9] F. Raupp-Pereira, A.M. Segadaes, A.S. Silva, J. Rocha, J.A. Labrincha, ^{27}Al and ^{29}Si NMR and XRD characterisation of clinkers: standard phases and new waste based formulations, Adv. Cem. Res. 107 (1) (2008) 37–45.
[10] P.S. Whitfield, L.D. Mitchell, Quantitative Rietveld analysis of the amorphous content in cements and clinkers, J. Mater. Sci. 38 (2003) 4415–4421.
[11] T. Westphal, G. Walenta, M. Gimenez, E. Bermejo, T. Fullmann, K.L. Scrivener, H. Pöllmann, Characterisation of cementitious materials, International Cement Review—Process Control, 2002.
[12] A.R. Brough, A. Atkinson, Sodium silicate-based, alkali-activated slag mortars: part I. strength, hydration and microstructure, Cem. Concr. Res. 32 (6) (2002) 865–879.
[13] A.R. Brough, A. Atkinson, Automated identification of the aggregate–paste interfacial transition zone in mortars of silica sand with Portland or alkali-activated slag cement paste, Cem. Concr. Res. 30 (6) (2000) 849–854.
[14] E. Demoulian, C. Vernet, F. Hawthorn, P. Gourdin, Slag content determination in cements by selective dissolution, Proceedings of the 7th International Congress on the Chemistry of Cement, Paris, France, 1980, pp. 151–156, II, III.
[15] V.F.J. Levelt, E.B. Vriezen, R.V. Galen, Determination of the slag content of BFS cements by means of a solution method, Zem. Kalk Gips 35 (2) (1982) 96–99.
[16] F.P. Glasser, D.E. Macphee, E.E. Lachowski, Solubility modelling of cements: implications for radioactive waste immobilisation, Mater. Res. Soc. Symp. Proc. 84 (1987) 331–341.
[17] K. Luke, F.P. Glasser, Selective dissolution of hydrated blast furnace slag cements, Cem. Concr. Res. 17 (2) (1987) 273–282.
[18] A.F. Battagin, Influence of degree of hydration of slag on slag cements, Proceedings of the 9th International Congress on the Chemistry of Cement, New Delhi, India, 1992, pp. 166–172, III, II.
[19] J.S. Lumley, R.S. Gollop, G.K. Moir, H.F.W. Taylor, Degrees of reaction of the slag in some blends with Portland cements, Cem. Concr. Res. 26 (1) (1996) 139–151.
[20] J.I. Escalante, L.Y. Gomez, K.K. Johal, G. Mendoza, H. Mancha, J. Mendez, Reactivity of blast-furnace slag in Portland cement blends hydrated under different conditions, Cem. Concr. Res. 31 (10) (2001) 1403–1409.
[21] M. Regourd, B. Mortureux, E. Gautier, H. Hornain, J. Volant, Characterisation and thermal activation of slag cements, Proceedings of the 7th International Congress on the Chemistry of Cement, Paris, France, 1980, pp. 105–111, II, III.
[22] Y. Totani, Y. Saito, M. Kageyama, H. Tanaka, The hydration of blast furnace slag cement, Proceedings of the 7th International Congress on the Chemistry of Cement, Paris, France, 1980, pp. 95–98, II, III.
[23] X. Wu, D.M. Roy, C.A. Langton, Early hydration of slag-cement, Cem. Concr. Res. 13 (2) (1983) 277–286.
[24] Geiker M., Studies of Portland cement hydration by measurements of chemical shrinkage, PhD thesis, Technical University of Denmark, 1983.
[25] Dyson H.M., Early hydration in binary and ternary blended cement systems, PhD thesis, University of Leeds, 2005.
[26] H.F.W. Taylor, K. Mohan, Analytical study of pure and extended Portland cement pastes: I, pure Portland cement pastes, J. Am. Ceram. Soc. 68 (12) (1985) 680–685.
[27] K. Luke, F.P. Glasser, Internal chemical evolution of the constitution of blended cements, Cem. Concr. Res. 18 (4) (1988) 495–502.
[28] H. Dyson, I. Richardson, A.R. Brough, A combined ^{29}Si MAS NMR and selective dissolution technique for the quantitative evaluation of hydrated blast furnace slag cement blends, J. Am. Ceram. Soc. 90 (2) (2007) 598–602.
[29] R. Goguel, A new consecutive dissolution method for the analysis of slag cements, Cem. Concr. Aggregates 17 (1) (1995) 84–91.
[30] W. Schrämli, Characterisation of blastfurnace slags by means of differential thermal analysis, Zem. Kalk Gips 4 (1963) 140–147.
[31] J.E. Krüger, M.S. Smit, Endothermal DTA peak preceding exothermal devitrification peak for vitreous blast-furnace slag, Cem. Lime Manuf. 42 (4) (1969) 77–80.
[32] R. Sersale, G. Frigione, Microstructure and properties of hydrated cements with different slag content, Proceedings of the 7th International Congress on the Chemistry of Cement, Paris, France, 1980, pp. 63–68, II, III.
[33] W. Hinrichs, I. Odler, Investigation of hydration of Portland blastfurnace slag cement: hydration kinetics, Adv. Cem. Res. 5 (2) (1989) 9–13.
[34] A.A. Francis, Non-isothermal crystallisation kinetics of a blast furnace slag glass, J. Am. Ceram. Soc. 88 (7) (2005) 1859–1863.
[35] C. Fredericci, E.D. Zanotto, E.C. Ziemath, Crystallization mechanism and properties of a blast furnace slag glass, J. Non-Cryst. Solids 273 (1–3) (2000) 64–75.
[36] O.V. Mazurin, Problems of compatibility of the values of glass transition temperatures published in the world literature, Glas. Phys. Chem. 33 (1) (2007) 22–36.
[37] Van Rompaey G., Etude de la réactivité des ciments riches en laitier, à basse température et à temps court, sans ajout chloruré, PhD thesis, Université Libre de Bruxelles, 2006
[38] V.S. Ramachandran, R.M. Paroli, J.J. Beaudoin, A.H. D., Handbook of Thermal Analysis of Construction Materials, Noyes Publications, William Andrew publishing, Norwich, New York, U.S.A, 2002.
[39] K.L. Scrivener, H.H. Patel, P.L. Pratt, L.J. Parrott, Analysis of Phases in Cement Paste using Backscattered Electron Images, Methanol Adsorption and Thermogravimetric Analysis in Microstructural Development during the Hydration of Cement, Proceedings of Material Research Society Symposium, 85, 1987, pp. 67–76.
[40] M. Mouret, E. Ringot, A. Bascoul, Image analysis: a tool for the characterisation of hydration of cement in concrete — metrological aspects of magnification on measurement, Cem. Concr. Compos. 23 (2–3) (2001) 201–206.
[41] W. Hansen, Y. Peng, C. Borgnakke, Y. N., J.J. Biernacki, Pozzolanic reactivity of ground granulated blast furnace slag in blended cement, Proceedings of the 2nd International Symposium on Advances in Concrete through Science and Engineering, Quebec City, Canada, 2006.
[42] Y. Peng, W. Hansen, C. Borgnakke, J.J. Biernacki, Hydration kinetics of Portland cement containing Supplementary Cementitious Materials (SCMs), Journal of American Ceramic Society, Special Volume High-Performance Cement-Based Composites, 2005, pp. 149–164.
[43] Costoya M., Effect of particle size on the hydration kinetics and microstructural development of tricalcium silicate, PhD thesis, Ecole Polytechnique Fédérale de Lausanne, 2008.
[44] L. Wadsö, Notes from Nanocem Calorimetry Workshop, Building Materials Lund University, Sweden, October 2006.
[45] D.P. Bentz, Transient plane source measurements of the thermal properties of hydrating cement pastes, Mater. Struct. 40 (10) (2007) 1073–1080.
[46] J.P. Holman, Heat Transfer, ed, McGraw-Hill, New York, 1981.
[47] S.S. Todd, Low temperature heat capacities and entropies at 298.16°K of crystalline calcium orthosilicate zinc orthosilicate and tricalcium silicate, J. Am. Chem. Soc. 73 (1951) 3277–3278.
[48] M. Ben Haha, K. De Weerdt, B. Lothenbach, Quantification of the degree of reaction of fly ash, Cem. Concr. Res. 40 (11) (2010) 1620–1629.
[49] W.A. Gutteridge, On the dissolution of the interstitial phases in Portland cement, Cem. Concr. Res. 9 (3) (1979) 319–324.
[50] W. Sha, E.A. O'Neill, Z. Guo, Differential scanning calorimetry study of ordinary Portland cement, Cem. Concr. Res. 29 (9) (1999) 1487–1489.
[51] T. Kishi, K. Maekawa, Thermal and mechanical modelling of young concrete based on hydration process of multi-component cement minerals, International RILEM Symposium, 1994.
[52] T. Kishi, Personal Communication, 2009.
[53] R. Grün, K. T., G. Kunze, Messung der latenten Energie von Hochofensschlacken und von Einzelkomponenten des Dreistoffsystems Kieselsaüre-Kalk-Tonerde-2, Zement, 1925.
[54] R. Grün, K. T., G. Kunze, Messung der latenten Energie von Hochofensschlacken und von Einzelkomponenten des Dreistoffsystems Kieselsaüre-Kalk-Tonerde-1, Zement, 1925.
[55] S.L. Poulsen, H.J. Jakobsen, J. Skibsted, Methodologies for Measuring the Degree of Reaction in Portland Cement Blends with Supplementary Cementitious Materials by ^{27}Al and ^{29}Si MAS NMR Spectroscopy, Proceedings of 17th IBAUSIL — Internationale Baustofftagung, Weimar, Germany, 1, 2009, pp. 117–188.
[56] Poulsen S.L., Methodologies for measuring the degree of reaction in Portland cement blends with supplementary cementitious materials by ^{29}Si and ^{27}Al MAS NMR spectroscopy, PhD thesis, Aarhus University, Denmark, 2009